J Ther Eng, Vol. 11, No. 1, pp. 94−111, January, 2025

Journal of Thermal Engineering
Web page info: https://jten.yildiz.edu.tr
DOI: 10.14744/thermal.0000906

Research Article

Modeling and co-simulation of an integrated solar heating system and direct contact membrane distillation module

Mouad BOUSMAHA[1,2,*], Ahmed REMLAOUI[2], Driss NEHARI[2]

[1]*Smart Structure Laboratory, University of Ain Témouchent, Ain Témouchent, 46000, Algeria*
[2]*Applied Hydrology and Environment Laboratory, University of Ain Témouchent, Ain Témouchent, 46000, Algeria*

ARTICLE INFO

Article history
Received: 23 September 2023
Revised: 16 March 2024
Accepted: 15 April 2024

Keywords:
Co-simulation; Desalination; Direct Contact Membrane Distillation; Solar Heating

ABSTRACT

This study investigates the use of a solar heating system and a direct contact membrane distillation module to produce pure water. The study employs co-simulation techniques that combine TRNSYS and MATLAB. The integrated system consists of a flat sheet membrane module for purification, a hot water storage tank with an internally regulated auxiliary heater, and a flat plate collector for thermal energy supply. A novel membrane distillation module was used, allowing the liquid to make direct contact with the membrane. The module was developed in MATLAB, reprogrammed, and then integrated into the TRNSYS framework. The TRNSYS-MATLAB co-simulation assessed the integrated system's long-term efficiency. This novel solar desalination technique also improves prediction flexibility for various membrane distillation scales and configurations (such as co-current and counter-current). The current study used and validated the use of Polyvinylidene fluoride flat sheet membrane distillation in both co-current and counter-current arrangements at small and large scales, comparing the results to previously published research. Increasing the collector area from 2 m^2 to 8 m^2 in Ain Témouchent's weather conditions reduces the auxiliary heating rate by 14% in December and 44.27% in August. In the summer, solar fraction and solar collector efficiency are 71% and 63%, respectively. The current integrated system can collect approximately 54.28 l of water flux through the membrane per day, resulting in a membrane production rate of 13.57 kg/m^2.hr. The findings show that the use of modern co-simulation techniques is highly inventive, producing environmentally friendly water in a sustainable and efficient way.

Cite this article as: Bousmaha M, Remlaoui A, Nehari D. Modeling and co-simulation of an integrated solar heating system and direct contact membrane distillation module. J Ther Eng 2025;11(1):94−111.

INTRODUCTION

Potable water scarcity has become more severe in Mediterranean countries and other regions around the world in recent years as demand and population growth put pressure on natural water sources [1]. Although water covers more than two-thirds of the planet, 99.3%

***Corresponding author.**
*E-mail address: mouad.bousmaha@univ-temouchent.edu.dz, bousmahamouad@gmail.com

This paper was recommended for publication in revised form by Editor-in-Chief Ahmet Selim Dalkılıç

is either too salty or unavailable for human consumption [2].

Solar distillation was the first technology used until now to produce pure water from solar energy. Tiwari et al. [3, 4] recently attempted to improve this technique; however, despite all efforts by researchers and engineers, the production of drinking water from this technique is insufficient to meet the constantly increasing demand. Reverse osmosis (RO) technology was developed in 1959 at the University of California and industrialized in the 1970s. Unlike solar distillation, RO produces a large quantity of fresh water while consuming much electricity due to the greed of powerful pumps. On the other hand, membrane distillation (MD) is a promising technique that operates at lower temperatures, typically between 50°C and 90°C [5], making it cooler than conventional distillation and operating at significantly lower pressures than the RO process [6, 7].

MD is a method of separating water that combines thermal distillation with a microporous hydrophobic membrane. The latter is used to extract water vapor from a heated aqueous solution (feed), resulting in a separation process caused by vapor pressure differences between the porous hydrophobic membrane surfaces [8]. The MD system's major processes are organized into three stages. The vapor gap is initially formed at the interface of the supply solution and the membrane. The vapor then passes through a hydrophobic membrane before condensing on the cold side of the permeable solution and membrane [9, 10].

Most MD studies now use commonly available microporous membranes such as polytetrafluoroethylene (PTFE) and polyvinylidene fluoride (PVDF) [11, 12], as well as thermally rearranged poly benzoxazole-co-polyimide (TR-PBOI), which was used in Kim et al.'s [6] membrane distillation study. Most MD modules have employed flat sheet and hollow fiber membrane geometries [13-15]. The first modules are easier to build and cleaner than the second modules, but they have a lower packing density [9]. Several layers of flat sheet membranes can be stacked on top of one another to increase the active membrane area. Damaged membranes are easily removed, so they are used in laboratory and industrial-scale applications [16].

The primary module configurations changed based on the permeate-side vapor condensation process: (1) Direct contact membrane distillation (DCMD): In this method, the vapor that passes condenses after mixing with the permeate solution on the permeate side. (2) Air-gap membrane distillation (AGMD): To reduce heat loss, stagnant air circulates between the membrane and the cold side, with water vapor condensing on the condensation side. (3) Vacuum membrane distillation (VMD): A vacuum pump creates a vacuum on the cold side, and water vapor condensation occurs outside the module. (4) Sweeping gas membrane distillation (SGMD): An inert gas is inserted to reduce heat loss and increase the coefficient of mass transfer, and the gas sweeps the vapor on the cold side, condensing it outside the module [17]. DCMD has received the most attention among the previously mentioned configurations due to its simplicity, the lack of external devices required for permeate condensation, and the fact that it has a very high permeation flux, making it suitable for water-based applications [18].

Desalination technologies powered by renewable energy sources can significantly alleviate water scarcity while minimizing negative environmental impacts [19]. However, due to MD's low feed temperature requirements, such as solar energy [20], which is consistently abundant in areas with a scarcity of freshwater, it appears to be a viable solution to this problem [21], making it suitable for the MENA region, particularly Algeria, which has a significant solar energy potential [22]. The combination of solar and desalination units provides clean water to remote areas without water or electricity [14]. Several experimental studies have been conducted to assess the feasibility of desalination applications using MD systems and solar energy on both a small and large scale.

In small-scale studies, Shim et al. [23] investigated the feasibility of using solar energy for saltwater desalination. They found that combining a DCMD module with a solar collector with a 4.7 m^2 flat plate collector (FPC) area and a 0.06 m^2 DCMD module area resulted in lower thermal efficiency. In this regard, several experimental studies have been carried out; one of these investigations is the SMADES project, which includes two small-scale pilots. The first model, built and tested in Irbid, Jordan [24, 25], has a 5.73 m^2 solar FPC area that directly heats the hot solution for an AGMD module with a ten m^2 membrane area. The system produces 19 l/m^2 of FPC area per day. The second pilot in Alexandria, Egypt [26] produced 11.2 l/m^2 of FPC area per day. In Aqaba, Jordan, two subsystems [27] were installed for the same project, including a 72 m^2 FPC field and a 40 m^2 AGMD system with heat recovery. A heat exchanger connected the two subsystems, with the desalination subsystem providing 2-11 l/m^2 of solar collector.

As for large-scale studies, a combined unit for saltwater desalination was built, with productivity ranging from 59 to 117 l/day on sunny days In PozoIzquierdo-Gran, Canary Island, Spain. The unit included an 8.5 m^2 permeation gap membrane distillation (PGMD) system area and internal heat recovery, linked to a 6.96 m^2 FPC area [28]. Selimli et al. conducted experiments on seawater distillation using a solar pond and a solar vacuum tube, demonstrating its environmental friendliness, cost-effectiveness, and efficiency. The solar tube increased heat energy, increased distilled water production, and required no additional energy, providing a promising and sustainable solution to water scarcity in low-energy areas [29]. In Almeria, Spain [30], pilot-scale AGMD modules of 2.8 and 9 m^2 were connected to a 500 m^2 compound parabolic collector (CPC) via heat exchangers. The authors [30] emphasized the importance of heat recovery in improving the thermal efficiency and performance of desalination systems, as found on a small scale by Banat et al. [27], and suggested multi-staging as a practical solution. The Fraunhofer ISE research group

[31] created three MD plant prototypes, two of which are solar-powered and located in Amarika and Gran Canaria. The Amarika system included 12 AGMD modules with a total membrane area of 168 m^2 and 232 m^2 of solar FPC area, yielding 2.08 m^3/day. In contrast, the Gran Canaria system featured a 120 m^2 AGMD loop and a 186 m^2 FPC solar loop, producing 1.4 m^3 per day. The thermal energy flux analysis revealed that only 28% and 30% of solar radiation reached desalination plants in Amarika and Gran Canaria, respectively [31].

Comparing the results of small and large-scale studies is difficult due to differences in MD composition, unit size, membrane properties, and other variables. The reviewed studies [23-27] in the small-scale case show consistent daily distillate production of 10-30 l/m^2.hr of solar collector surface area. In terms of overall surface area, this production rate was lower than in traditional MD systems with a constant auxiliary heating source. Large-scale studies revealed that significantly more energy was used than was produced on a daily basis. To address these issues and improve productivity, the researchers believed that creating a comprehensive productivity forecasting simulation would be preferable.

Nowadays, significant advances in computational sciences enable us to improve overall system design through numerical modeling, as demonstrated by several open-source and commercial codes. Recently, Dong et al. [32] used a "tanks-in-series" mathematical model [33, 34]. This mathematical method accurately predicted steady-state membrane desalination for the flat sheet DCMD configuration using laboratory-scale experimental data from a single configuration. These data were used as simulation inputs to determine the permeation coefficient C_m for the membrane material used. Once this coefficient is determined, it is possible to model different DCMD configurations with identical physical characteristics but different orientations (co-current and counter-current), dimensions, and operating conditions. Dong et al. [32] validated this method experimentally for PVDF and TR-PBOI, obtaining mass fluxes of 38.8 kg/m^2 and 88.9 kg/m^2.s, respectively.

Depending on the plant's characteristics, solar energy can be used for thermal or photonic desalination or both. These effects could be represented using thermal solar collectors or photovoltaic panels (PV) to generate fresh water using the MD technique. In thermal collectors, the heat transfer fluid HTF, which could be water, glycols, nanofluids, or a hybrid, is used, depending on the required level of thermal efficiency [36].

In recent years, engineers and researchers have worked hard to model solar desalination on both small and large scales. Ain Témouchent, Algeria's research group, conducted empirical studies and simulations of solar-powered MD systems. Remlaoui, Nehari et al. [37] used TRNSYS simulation to validate the integration of solar thermal (FPC) and photovoltaic (PV) energy powering DCMD to produce clean water, and the DCMD unit was added as a new FORTRAN component that was linked to the two solar systems. On the chosen day, the suggested system generated approximately 59.34 l/day, with a collector efficiency of 64%, as measured by the FPC value. (June 24). Marni, Nehari, et al. [38] recently investigated an AGMD simulation with TRNSYS, which included a quadratic polynomial model regression analysis of experimental results. The proposed system reduces carbon dioxide emissions by 7274.45 kg/year and produces 28.78 m^3/year of drinking water at a cost of USD 14.73 per m^3.

Hogan et al. [39] used solar-heated saline water to feed membrane distillation (MD) systems. The system had a total area of 1.8 m^2 hollow fibers, 1.8 m^2 FPC, and 0.7 m^2 heat exchange. It was simulated with the TRNSYS program, and the results showed that productivity reached 50 kg/day, which is sufficient for domestic pure water requirements. Recent research using TRNSYS software predicted a small-scale FPC-driven DCMD system with daily production values of 19.7 kg/m^2 MD and 6.3 kg/m^2 FPC [40]. Furthermore, as the feed flow rate increased, the distilled water flux and thermal efficiency decreased unexpectedly, contradicting the results of standard DCMD modules. The authors attributed this to higher flow velocities, shorter feed residence time within the thermal collector, and lower feed input temperatures.

The TRNSYS software is commonly used to treat solar systems. This is a powerful tool for simulating thermal and electrical systems over time. TRNSYS can be used alongside other software to model more complex systems, but it cannot predict desalination processes. On the other hand, the literature clearly shows that desalination processes are well-written in coding languages (MATLAB, FORTRAN, C...). Combining TRNSYS with a coding language will enable us to simulate solar desalination dynamically. MATLAB is more flexible than other languages in terms of co-simulation with TRNSYS for a variety of physical phenomena. As is well known, the co-simulation tool MATLAB-TRSYS can be used in a variety of calling modes, including non-steady states [41].

According to the studies presented above, thermal collectors are primarily used to feed seawater into the MD at an acceptable temperature range (50-80°C). Many studies [6,37,38,40] attempted to simulate a system that combined solar thermal energy and an MD module. The approach proposed in this study overcomes the shortcomings of prior research by introducing a novel numerical modeling and simulation method for integrated solar desalination systems. Past research has mainly concentrated on modeling either the membrane by itself or the steady-state membrane along with solar systems, which has restricted the ability to explore different configurations. We are using a new simulation method that combines time marching and TRNSYS-MATLAB co-simulation to analyze system parameters in real-time for solar desalination. Our method improves the flexibility of the co-simulation across various scales and MD configurations by utilizing the benefits of the DCMD model, enabling a more thorough analysis of

system performance in different scenarios. This novel concept must be considered in solar desalination based on our understanding. The second goal is to enhance the adaptability of the co-simulation to various scales and MD configurations by utilizing the advantages of the DCMD model over other solar desalination modeling techniques.

MATERIALS AND METHODS

This study primarily aims to operate self-contained desalination units using renewable energy. Figure 1a depicts the use of direct contact membrane distillation (DCMD) and a flat plate collector (FPC) to extract freshwater from seawater. The system consists primarily of two major loops: solar heating and membrane distillation.

Solar Heating Subsystem

The solar subsystem consists of two components: the solar field and thermal storage. The solar field consists of a network of solar collectors connected to an insulated hot storage tank with an auxiliary heater. A flat plate collector captures sunlight and converts it to thermal heat. The HTF collects thermal energy from the FPC and transfers it

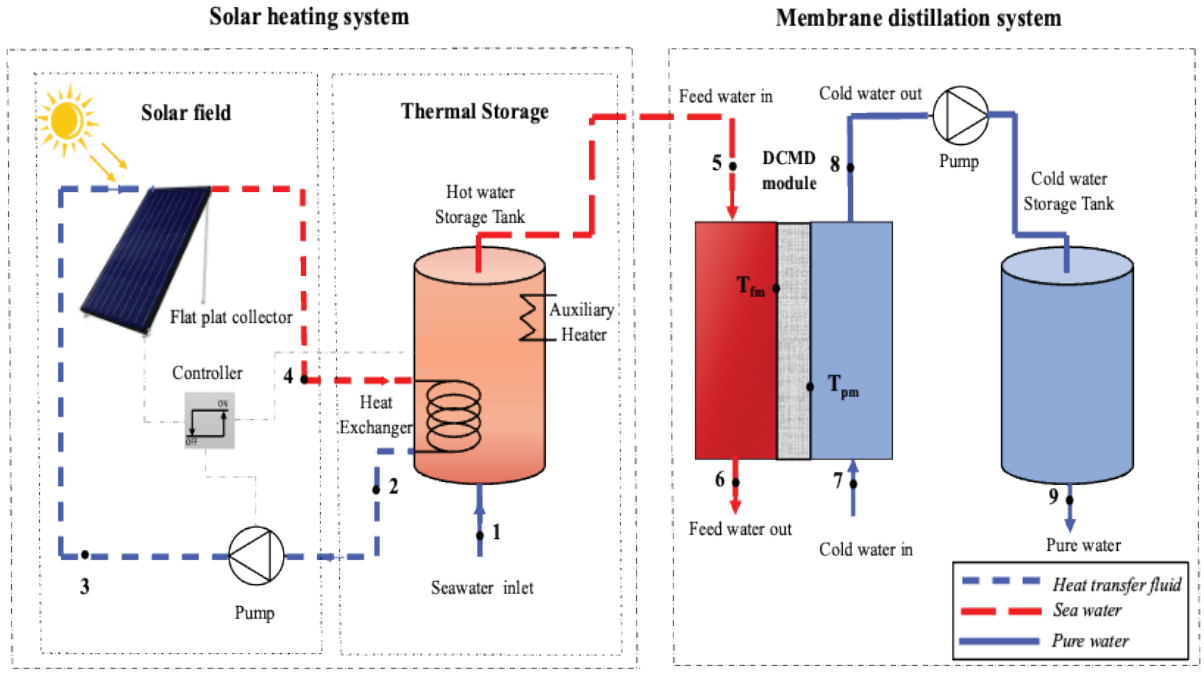

(a)

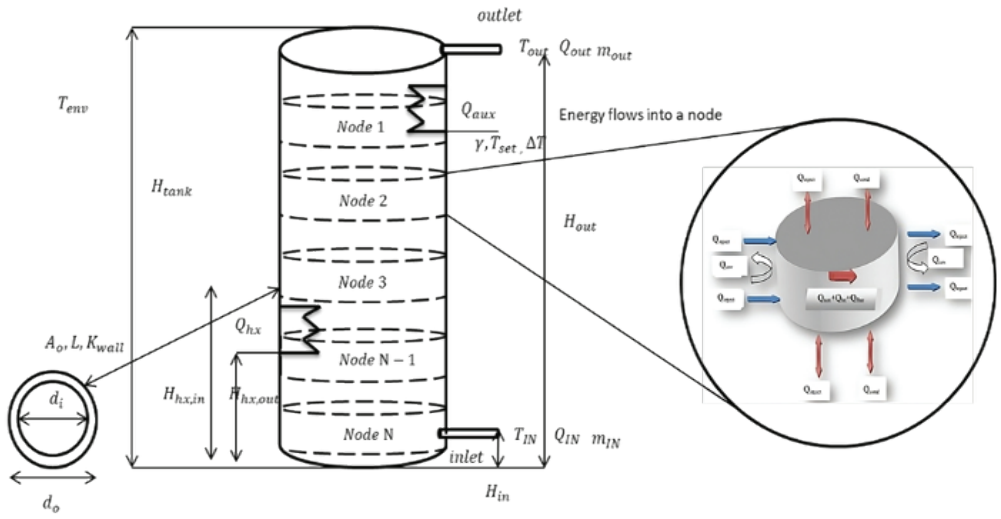

(b)

Figure 1. Schematic overview of the integrated system. (a) DCMD module and solar heating system, (b) Stratified hot water storage tank.

to the hot part of the DCMD module using the solar heating system [42]. The storage tank, which uses a coil heat exchanger, allows for the exchange of seawater and HTF; the heat transfer fluid used in this study is glycol. The system also includes an optional electric resistance-heating element with a heater and thermostat to regulate the hot water temperature. The flat plate collector functions as a heat exchanger, converting solar energy into thermal energy that is communicated to the HTF in circulation. To simulate this component, Type1b of TRNSYS was employed. The useful thermal energy (Qu) gained from irradiation to the HTF is a widely used parameter for assessing the performance of this type of collector [43, 44].

$$Q_u = \dot{m}_{HTF}.Cp_{HTF}.(T_3 - T_4) \quad (1)$$

where, Q_u signifies the heat collected via the FPC (kJ/hr), T_3 and T_4 are, respectively, the HTF's inlet and outlet temperatures (K), $\dot{m}_{HTF}$ is the HTF's mass flow rate (kg/hr), and Cp_{HTF} is the HTF's specific heat capacity (kJ/kg. K)

In addition to useful thermal energy, solar collector efficiency is an effective way to assess FPC performance. It can be written as: [37].

$$\eta_{coll} = \frac{Q_u}{A_{SC}.I_T} \quad (2)$$

where, A_{SC} is the FPC area (m^2), and I_T is the total incident solar radiation (kJ/hr.m^2).

The hot water storage tank contains an internal heat exchanger (internal coil) and an auxiliary heater that provides the energy needed to reach the desired temperature. To determine the energy exchanges within this tank, which is divided into several layers (nodes) as shown in Figure 1b, we used the energy equation at each node based on the literature [45,46]:

$$M_i C_p.\frac{dT}{dt_i} = Q_{conve} + Q_{condu} + Q_{hx} + Q_{aux} + Q_{inject} \quad (3)$$

This equation includes the heat convection between the storage tank and the ambient air Q_{conve}, conduction transmitted through the tank's metal Q_{condu}, energy gained from the solar system by heat exchanger Q_{hx}, the energy produced by the auxiliary heater Q_{aux}, forced convective heat transfer from or to the segments above and below Q_{inject}. The M_i (kg) and C_p (kJ/kg. K) are, respectively, the mass and the specific heat of seawater. It is worth noting that each Q equation has been precisely expanded on in the literature, which aligns with the general equation used in this study [45, 46]. Moreover, it is well known that the solar fraction (S_F) is an important thermal system performance parameter. It is defined as a relation between the energy delivered by the solar collector (Q_u) and the total quantity of solar energy required to operate the system (Eq. 4) [47]:

$$S_F = \frac{Q_u}{Q_u + Q_{aux}} \quad (4)$$

Membrane Distillation Subsystem

The DCMD module is divided into two additional loops (feed water loop and permeate water loop), as shown in Figure 1a. The feed water loop introduces hot saltwater from the storage tank directly into the feed side of a hydrophobic membrane; in contrast, the permeate water loop pumps fresh water and mixes it with permeate water that has passed through the membrane pores. The freshwater from the DCMD system is collected, and the brine is released into the sea. Because mathematical modeling is one of the necessary tools for evaluating the thermophysical performances of such systems, the model of Dong et al. [32] is well adopted in the current study, owing to its accuracy in predicting such phenomena as well as its good quality in terms of flexibility and application from small to large scales. This model works under the following conditions: the membrane can completely reject salt without wetting, the membrane module is well insulated, the transfer phenomena are in a steady state, and the effects of fluid entry and exit of the membrane are ignored.

In this study, only the flat sheet DCMD module of Dong et al. [32] was used, re-coded in MATLAB, and thoroughly tested against the same authors' experimental results. This model uses laboratory test results as inputs to estimate the performance of scaled-up MD systems in various configurations (co-current and counter-current), as shown in Figure 2a. The final modeling step used tanks-in-series, a mathematical approach, to simulate membrane separation. This method divides the membrane into multiple tanks of equal lengths. Figure 2b depicts the heat and mass transfer across the membrane in the DCMD module.

An iterative method was used under both configurations to simulate mass transfer using equations from Eq. (5) to Eq. (7) and heat transfer using equations from Eq. (8) to Eq. (14). The driving force of mass transfer is determined by vapor pressure changes inside the dry porous membrane and the membrane water flux can be expressed using the following equation [23]:

$$J_i = A_i.C_m.\Delta P^{sat} = A_i.C_m\left(P'^{sat}_{fm,i} - P^{sat}_{pm,i}\right) \quad (5)$$

The permeability coefficient of the membrane, denoted as C_m, is an important metric determined by the membrane's microstructural properties. Dong et al. [32] used the same method to calculate C_m using laboratory-scale experimental data. This method can predict the large-scale performance of units with a similar membrane and identical C_m. Then, a new method for estimating water flux J of the scaled-up was used. This method, based on the tanks-in-series approach, predicts the J iteratively. Raoult's law can be used to calculate the feed's partial vapor pressure in

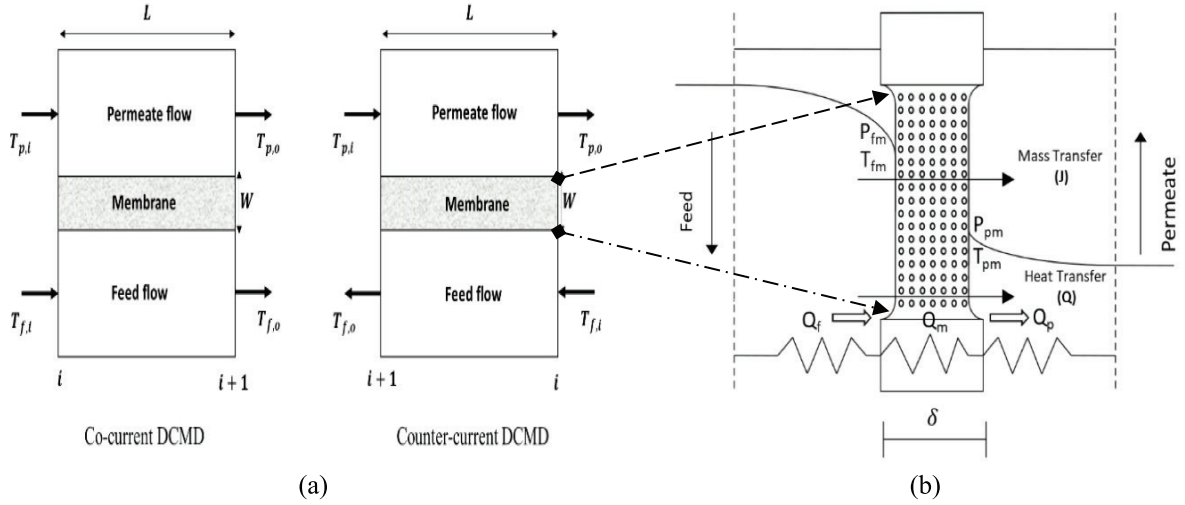

Figure 2. (a) Direct contact membrane distillation configurations, (b) Heat and mass transfer in DCMD module.

an aqueous NaCl solution, assuming 100% salt rejection on the feed side alone [48, 49].

$$P'^{sat}_{fm,i} = (1-x_{NaCl,i}) \cdot (1 - 0.5.x_{NaCl,i} - 10.x^2{}_{NaCl,i}).P^{sat}_{fm,i} \quad (6)$$

Water saturation pressure at the feed and permeate membrane sides, P^{sat}_{fm} and P^{sat}_{pm}, were evaluated using the Antoine equation at the feed and permeate temperatures $T_{fm,i}$ and $T_{pm,i}$, where $x_{NaCl,i}$ is the mole fraction of NaCl in the feed solution as mentioned in reference [50]:

$$P^{sat}_{m,i} = 133.322.10^{\left(8.07131-\left[\frac{1730.630}{T_{m,i}-39.724}\right]\right)} \quad (7)$$

On the other hand, the heat transfer in the DCMD module is divided into 3 regions:

(i) The convective heat transfer between the feed water and the membrane at the feed side is represented by Eq. (8):

$$Q_{f,i} = h_{f,i}(T_{5,i} - T_{fm,i}) \quad (8)$$

(ii)The total heat transfer through the membrane ($Q_{m,i}$) is at the same time by conduction ($Q_{c,i}$) and latent exchange generated by water vapor passage ($Q_{v,i}$) [51].

(iii) The conductive heat flow over the flat sheet membrane can be calculated using the following equation [36a]:

$$Q_c = \frac{A_i.k_{mem}}{\delta}.(T_{fm} - T_{pm}) \quad (9)$$

k_{mem} is the membrane thermal conductivity, can be calculated using the following equations.

$$k_{mem} = (1 - \varepsilon).k_p + \varepsilon.k_g \quad (10)$$

where, ε is membrane porosity and k_p, k_g are the thermal conductivity of the solid (polymer) and gas in pores, respectively.

$$Q_{m,i} = Q_{c,i} + Q_{v,i} = \frac{A_i.k_{mem}}{\delta}.(T_{fm} - T_{pm}) + J_i\Delta H_{v,i} \quad (11)$$

$\Delta H_{v,i}$ is the vaporation latent heat, given by Eq. (12) [9]:

$$\Delta H_{v,i} = 1.7535.T_i + 2024.3 \quad (12)$$

The convective heat transfer between the permeate and the membrane at the permeate side is represented by Eq. (13), as provided in reference [17]:

$$Q_{p,i} = h_{p,i}(T_{pm,i} - T_{7,i}) \quad (13)$$

where, $T_{5,i}$ and $T_{7,i}$ are the bulk temperatures on the feed and permeate sides, respectively.

The convective heat transfer coefficients ($h_{f,i}$ and $h_{p,i}$) involve evaluating the Nusselt numbers. $h_{f,i}$ and $h_{p,i}$ varies based on operating conditions, the two convective heat transfer coefficients can be calculated using Eq. (14).

$$h_i = \frac{N_u.k}{D_i} \quad (14)$$

where, k is the fluid thermal conductivity on the feed and the permeate side, D_i is the hydraulic diameter of the flow channel, and N_u is Nusselt number, which depends on regime flow (laminar or turbulent).

Dong et al. [32] summarized the correlations used to calculate the Nusselt number. The mathematical model was used to predict DCMD processes under a variety of operating conditions, as the temperature of the feed and permeate solutions, as well as the amount of NaCl in the feed, have a significant

impact on thermophysical parameters such as density-specific heat, thermal conductivity, and dynamic viscosity [32].

Dynamic Model (TRNSYS Simulation)

The TRNSYS software was used to design the proposed solar heating and membrane distillation system. Figures 3 and 4 show the system's primary components. The solar field system consists of meteorological data reading and processing (Type109-TMY2), a flat plate collector (Type 1b), a solar water pump (Type 3b), and a differential temperature controller (Type 2b). The thermal storage system consists of a stratified fluid storage tank (Type 60d) with optional internal heaters, internal heat exchangers with one input and output, and a general forcing function (Type 14h). Because the membrane distillation model is not available in TRNSYS, the previously created mathematical model of the DCMD flat sheet is used by calling an external application via MATLAB (Type 155). Table 1 summarizes the different parameter values for the FPC component used in this simulation. Table 2 lists the hot storage tank's main parameters, such as its dimensions and thermal characteristics. The DCMD model used in the simulation is an external component coded by MATLAB and called within TRNSYS; the main parameters, such as the number of inputs, outputs, and calling modes, are listed in Table 3. Table 4 shows the main operating conditions used for small-scale experimental validation based on literature

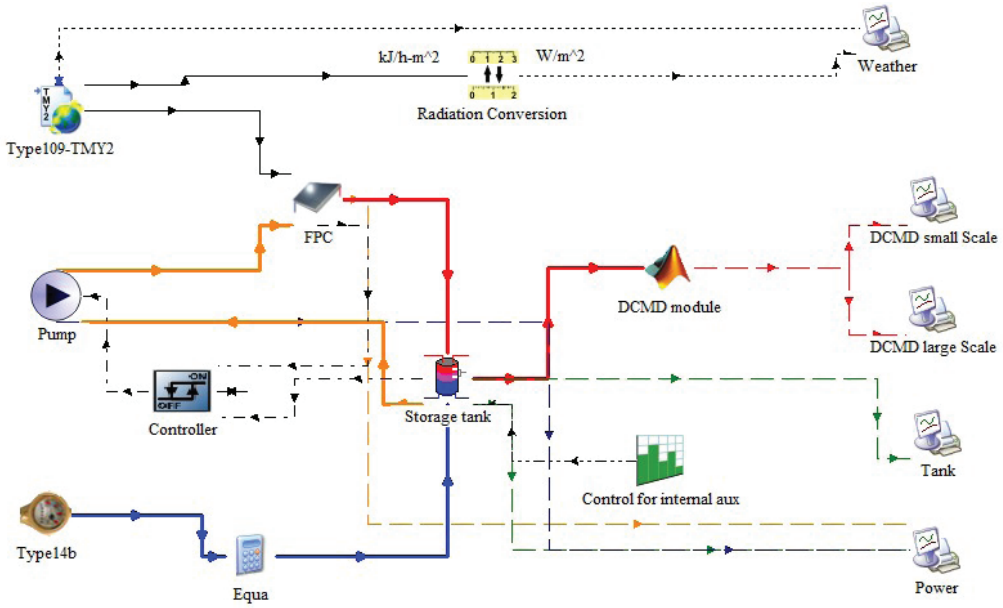

Figure 3. Complete TRNSYS model simulation.

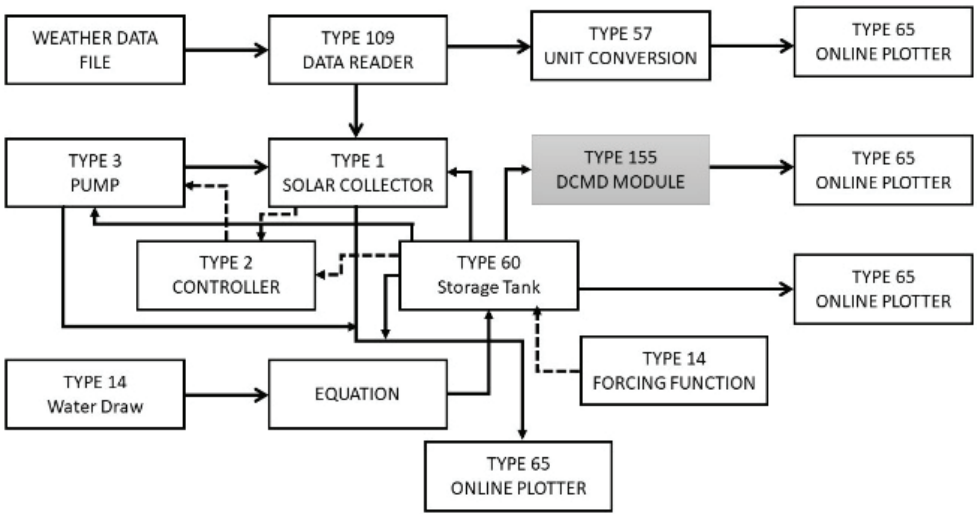

Figure 4. Workflow diagram including all components.

Table 1. Main parameters for FPC

Component (Type)	Parameters	Value	Unit
Flat plat collector (Type1b)	Collector area	2	m^2
	Specific heat of fluid	3.627	kJ/Kg.K
	Tested flow rate	40	Kg/hr.m^2
	Intercept efficiency	0.788	-
	Efficiency slope	4.15	W/m^2.K
	Efficiency curvature	0.017	W/m^2.K

Table 2. Main parameters for Hot water storage tank

Component (Type)	Parameters	Value	Unit
Hot water storage Tank (Type60d)	Volume	300	L
	Height	1.42	m
	Specific heat of fluid	3.911	kJ/kg.K
	Density of fluid	1040	Kg/m^3
	Thermal conductivity of fluid	0.6041	W/m.K
	Set point temperature for element 2	60	°C
	Fraction of glycol	0.5	-
	Heat exchanger length	32	m
	The total surface area of HX	1.2	m^2
	Wall conductivity of HX	390	W/m.K

Table 3. Main parameters for the DCMD system

Component (Type)	Parameters	Value
DCMD system (Type155)	Mode	0
	Number of inputs	22
	Number of outputs	20
	Calling Mode	0
	Keep Matlab open after the simulation	1

Table 4. Main operating conditions

Parameters	Value	Unit
Feed inlet NaCl concentration	35	g/kg
Feed inlet temperature	50-60	°C
Permeate inlet temperature	20	°C
Feed inlet mass flow rate	1	kg/s
Permeate inlet mass flow rate	1	kg/s

results [32]. Table 4 also includes our own set of operating conditions (for Ain Témouchent) that were used on a large scale.

MATLAB and TRNSYS can be used to model the entire system, including the solar heating and membrane distillation modules. TRNSYS is used to model the energy and solar system, and MATLAB is used to simulate the DCMD process. By combining both software, a more precise and effective model can be created, allowing for predictive control of various parameters such as feed and permeate inlet temperatures, feed and permeate flow rates, solar heating system efficiency, and DCMD system efficiency.

RESULTS AND DISCUSSION

This model was tested using weather data from Ain Témouchent. Figure 5 depicts the varying climatic conditions throughout the year. The weather in Ain Témouchent

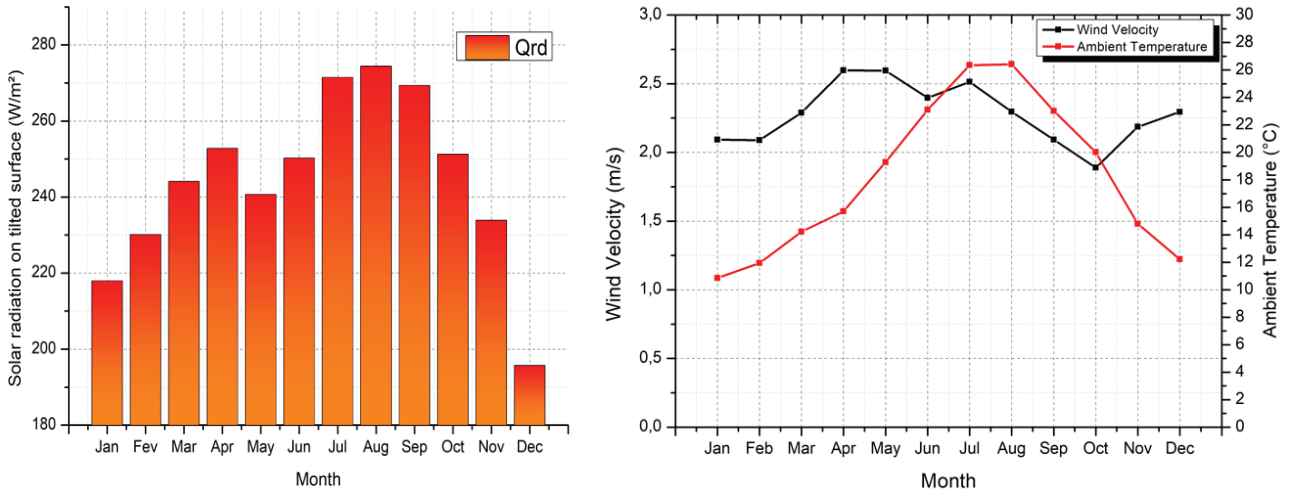

(a) (b)

Figure 5. Weather data in Ain Témouchent city. (a) Total radiation on a tilted surface, (b) Mean ambient temperature and wind velocity.

is typically pleasant, warm, and mild. During the winter months, solar energy decreases to a lower value, as illustrated in Figure 5a. Figure 5b depicts mean temperatures and wind velocity, with an average of 26.4 °C. August is the hottest month. The temperature varies throughout the year, peaking at 37°C in summer, with the highest recorded temperature of 36.35°C on July 21 and the coldest month being January, with an average of 10.8°C and the lowest temperature of 3.92°C on January 15. The wind is generally gentle, with a monthly average of 2.1-2.6 m/s, as illustrated in Figure 5b. Solar radiation fluctuates throughout the year, with the monthly average peaking at 274 W/m^2 during summer.

The current study used the same membrane and experimental input data as Dong et al. [32]. The permeation coefficient (C_m) for two materials, PVDF (38.8 kg/m^2.s) and TR-PBOI (88.9 kg/m^2.s), was calculated using the experimentally determined water flux (J). Furthermore, the study maintained the same properties of commercial membranes used in the MD process, such as porosity, thickness, thermal conductivity, and other related parameters, as described by Dong et al. [32]. After small-scale validation with a 0.5m^2 membrane area, a large-scale validation was performed using larger membrane areas to ensure model accuracy at different scales, validate large-scale temperatures, and allow direct comparison with Dong et al. [32]. We used data for a membrane area of 5 m^2, which corresponds to Dong et al.' temperature-related results (Figure 6). Dong et al.'s mass flux results ranged from 1 to 10 m^2, so we extended our analysis to a membrane area of 10 m^2 to fully compare the water flux results between the two studies (Figure 7).

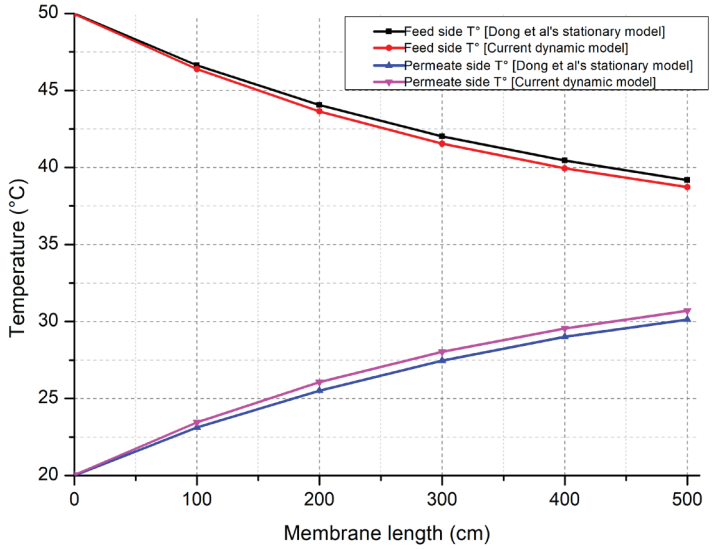

Figure 6. Comparison of temperature distributions of the feed and the permeate sides with Dong et al.'s model.

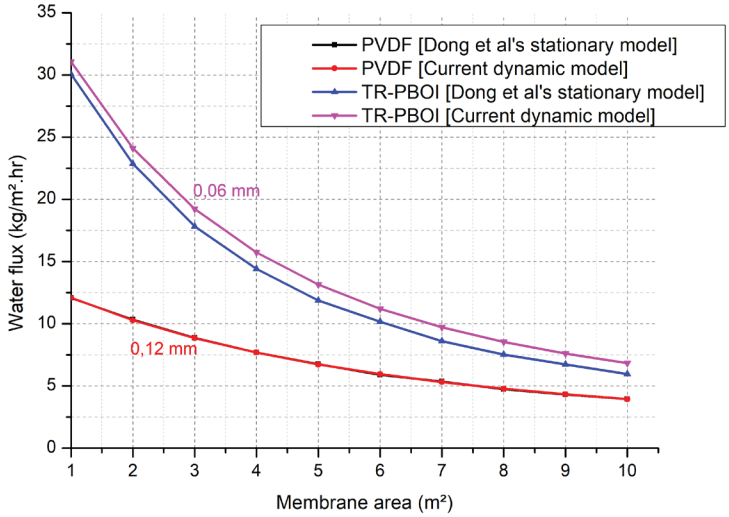

Figure 7. Large-scale validation for co-current DCMD model against Dong et al.'s model.

This plot compares water flux versus membrane area for PVDF and TR-PBOI membranes using Table 4's large-scale operational conditions and membrane areas ranging from 1 m^2 to 10 m^2. This figure provides a comprehensive understanding of the water flux behavior for the two materials; the results for PVDF material show good agreement, with a slight discrepancy of around 1% against Dong et al.'s model [32]. This figure shows an acceptable agreement for the TR-PBOI material, with an approximate 6% discrepancy. In both cases, the observed difference is minor and is due to the instantaneous effect considered in the current study. The PVDF membrane, which produces more accurate results, was used in the current study. Figure 6 depicts the temperature distributions on the feed and permeate sides of a co-current configuration with a 5 m membrane length, a 1m membrane width, one kg/s feed and permeate mass flow rates, and a salinity of 35 grams per kilogram. The results are in good agreement with Dong et al.'s [32]. Figure 6 shows temperature distributions in a co-current configuration with feed and permeate mass flow rates of 1 kg/s and salinity of 35 g/kg, as specified in Table 4. In this plot, we used the same operating parameters as in the previous large-scale validation, as shown in Figure 7. Our membrane area will range from 1 to 5 m^2, as validated against Dong et al.'s [32] values. As shown in Figure 6, the validation is in good agreement with the established literature model [32].

The DCMD model was run at 20°C for the permeate inlet and 70°C for the feed inlet, with a feed NaCl concentration of 30 g/kg. Table 5 compares the feed and permeate temperatures, as well as the water flux, of PVDF and TR-PBOI membranes obtained through the present modeling to those found experimentally by Dong et al. [32]. This comparison demonstrates good agreement and reveals that the temperature discrepancy is around 2%, while the flux does not exceed 1%. This good agreement demonstrates the accuracy of the current model.

The flat sheet membrane is suitable for both co-current and counter-current applications. The impact of these two configurations on water flux was assessed using a PVDF membrane. Figure 8 depicts the effect of membrane area on water flux in co-current and counter-current membrane configurations. Using the operating conditions listed in Table 4, the results show that for all membrane areas considered, the counter-current configuration provides more water flow than the co-current configuration, with the difference between these configurations increasing as the membrane area increases.

The integrated system results will be separated into two parts: the solar heating system and the DCMD module. As

Table 5. Small-scale validation results for mathematical DCMD model

Membrane properties	PVDF			TR-PBOI		
Results	**Experimental [32]**	**Current work**	**Error %**	**Experimental [32]**	**Current work**	**Error %**
Feed out temp (°C)	70.2	70.36	0.23	68.9	68.59	-0.45
Permeate out temp (°C)	19.8	19.52	-1.41	21.3	21.76	2.16
Water flux (Kg/m². h)	38.8	38.81	0.03	88.9	88.91	0.01

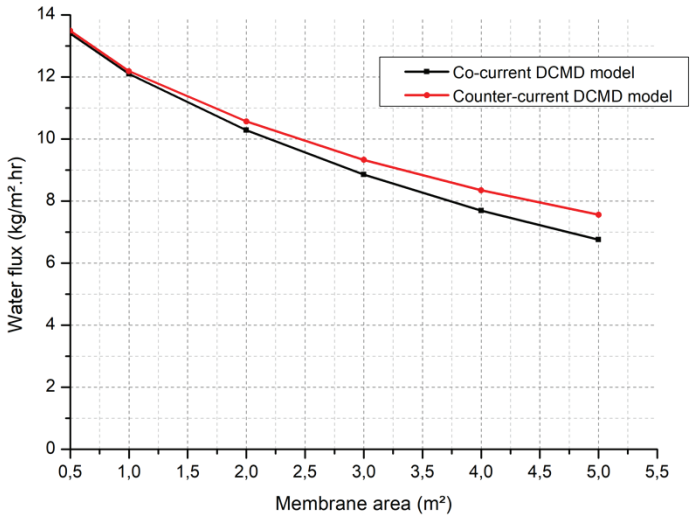

Figure 8. Predicted co - and counter-current water flux as a function of membrane area.

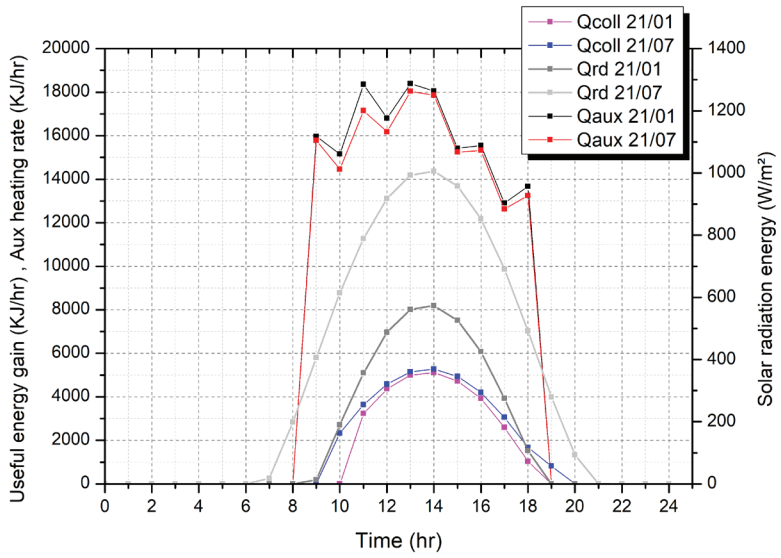

Figure 9. Solar radiation, energy provided by the FPC, and the auxiliary heating rate for definite days (January 21 and July 21).

is well known, the DCMD feed temperature ranges from 50° to 80°C. To investigate the solar part, we will use a feed temperature of 60°C to ensure that the membrane receives the necessary energy. Figure 9 shows the total radiation on the tilted surface (Q_{rd}), the useful energy gain (Q_u)to the HTF and the auxiliary heating rate supplied to the saltwater (Q_{aux}) over two significant days (January 21 and July 21). The plot shows that solar energy (Q_{rd}) peaks at 573 W/m² and 1006 W/m² during daylight on selected winter and summer days, respectively. The useful energy gain (Q_u) reaches its peak values of 5113 kJ/hr on January 21 and 5270 kJ/hr on July 21. This difference is due to seasonal variations in solar energy, as illustrated in Figure 9. The behavior of useful thermal energy (Q_u)is primarily determined by solar radiation. As a result, an apparent effect is observed, with summer months exhibiting correspondingly higher useful thermal energy values, as reported by Remlaoui et al. [37]. The plot shows that the auxiliary heating rate (Q_{aux}) is significant for both days, with nearly identical values. This value is due to their useful energy gain (Q_u) has similar behavior and values. As a result, the internal auxiliary heater primarily provides the energy required for the saltwater to reach the required temperature (60°C). This issue will be addressed below by expanding the flat plate collector area.

Figure 10 illustrates the monthly average of total radiation on the tilted surface (Q_{rd}), useful energy gain (Q_u), and auxiliary heating rate (Q_{aux}) for feeding saltwater at

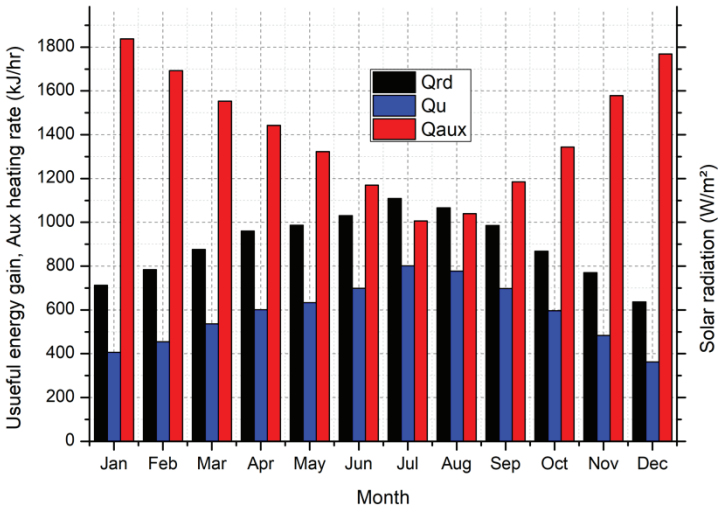

Figure 10. Solar radiation, energy provided by the FPC, and the auxiliary heating rate during the year.

60°C. As previously observed, this figure highlights the appearance of seasonal peaks in summer for both (Q_{rd}) and (Q_u). Conversely, the auxiliary energy requirement (Q_{aux}) decreases. These findings highlight the importance of sunlight's duration and intensity. According to that plot, the maximum order of the auxiliary heating rate is approximately 4.80 times the useful energy gain in December. In July, however, the minimum order is approximately 1.16. To address the previous issue, we attempted to increase the size of the thermal collector. Figure 11 shows the energy consumption of the auxiliary heater (Q_{aux}) for four collector areas (2, 4, 6, and 8 m²). This figure shows that the order of the auxiliary heating rate decreases as the surface area of the thermal collector increases, and it also depends on the strength and duration of solar radiation. For an 8 m² collector area, the auxiliary heating rate decreased by approximately 14% in December and by nearly 44.27% in August compared to a 2 m² collector area.

When solar radiation is at its peak, the collector achieves its maximum collector outlet temperature and useful thermal energy. Summer provides the highest output temperature and useful thermal energy values. In terms of thermal system performance, Figure 12 depicts how the collector's efficiency was evaluated over a year. Throughout the year, and based on Ain Témouchent's weather data, the monthly average of solar collector efficiency peaked in July at 64%. In comparison to the previous literature investigation [37], solar collector efficiency was recorded at 52% (January 24), 64% (June 24), and 55% (November 5). On the other hand, for the three selected days, the solar fraction was 41% (January 24), 52% (June 24), and 42% (November 5). This study evaluated the solar fraction of the thermal system

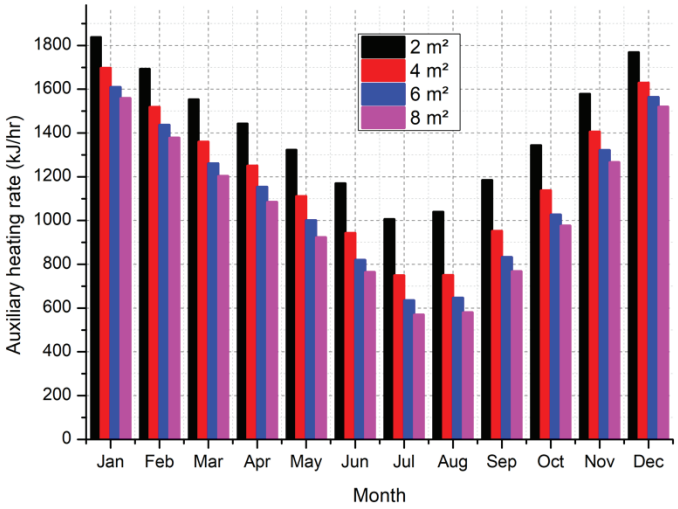

Figure 11. The auxiliary heating rate during the year for the different collector areas.

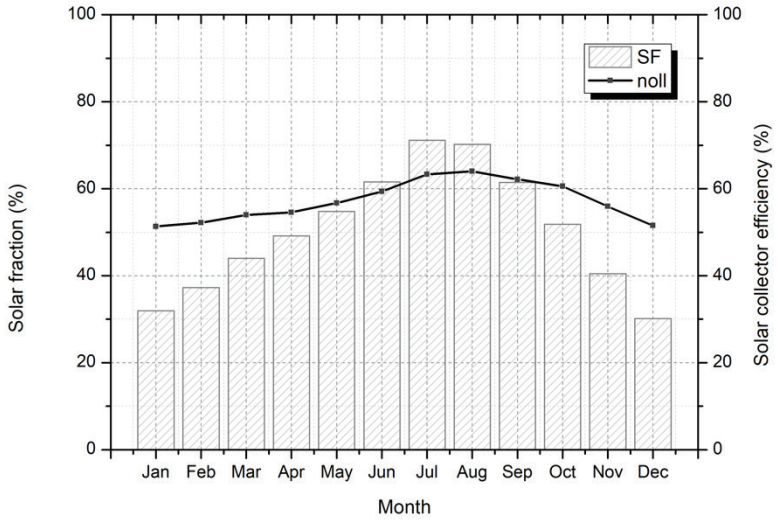

Figure 12. Monthly average solar fraction and solar collector efficiency.

over the year, as shown in the same figure, with a monthly average SF of 71% in July.

The module was tested under a variety of climatic conditions throughout the year for both co-current and counter-current configurations, with a feed temperature of 50°C from the hot storage tank. In contrast, the DCMD's cold inlet temperature is kept at 20°C, and the membrane length and width are 1 m and 0.5 m, respectively. Figure 13 shows the monthly water flux for two configurations: 50°C feed inlet, 20°C permeate inlet, and 0.5 m^2 membrane surface. We discovered that throughout the year, both counter-current and co-current configurations produced nearly identical water flow, with a difference of less than 1%. However, looking back at Figure 8, where we investigated various membrane surface areas, we noticed that this minor difference becomes more noticeable with larger surfaces. We used a 0.5 m^2 membrane in this analysis, so the two water flows are closely matched.

Figures 10-12 show that the solar thermal system performs best during the summer, particularly on July 21. On this day, we will examine the integrated system results (Figures 14 and 15). Figure 14 depicts the effect of feed inlet temperature on outlet feed and permeate temperatures, as well as water flux in the DCMD system. This investigation was carried out on July 21, with feed inlet temperatures ranging from 50°C to 80°C supplied by the hot storage tank. The results show that changes in feed inlet temperature have a direct impact on water flux. Higher feed inlet

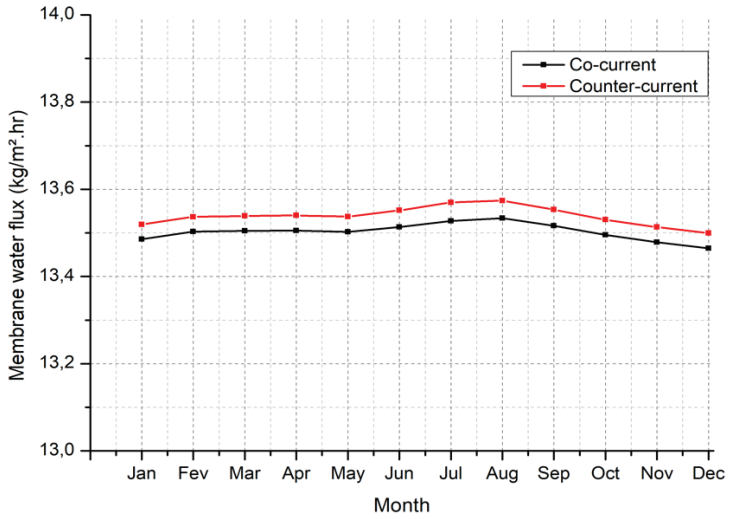

Figure 13. Membrane water flux in two configurations during the year for set feed inlet temperature 50°C, permeate inlet temperature: 20°C, membrane area: 0.5 m^2.

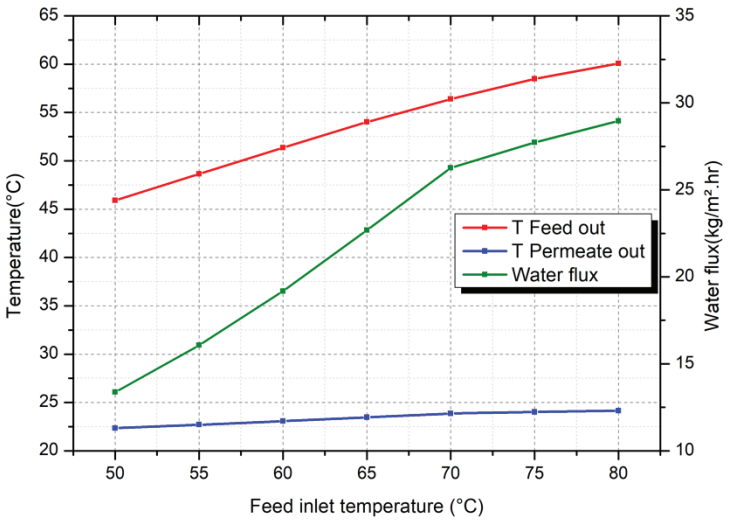

Figure 14. Feed temperature, permeate temperature, and membrane water flux versus set temperature in hot storage tank over the day (July 21).

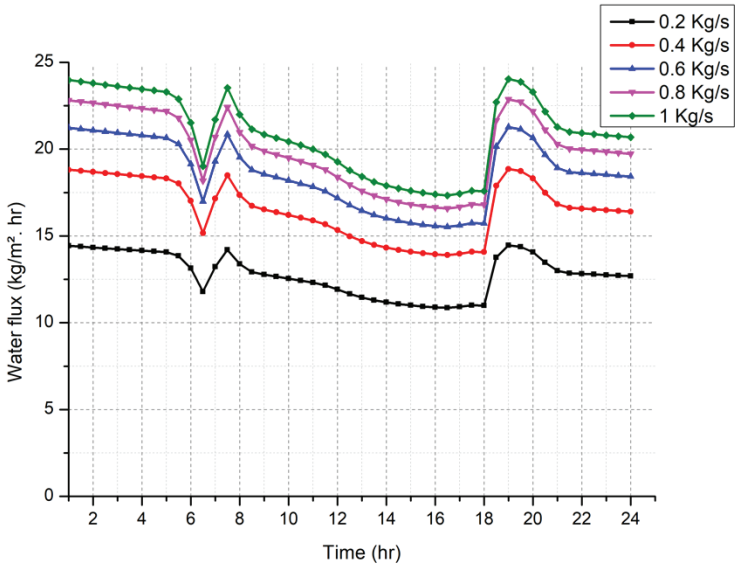

Figure 15. Membrane water flux over July 21 with different feed inlet mass flow rates.

temperatures, in particular, are associated with an increase in distilled water flux. Figure 14 shows that the exit temperature on the feed side varies from 45.89°C to 60.08°C, indicating the effect of various settings in the hot water storage tank. On the permeate side, temperatures range from 22.35°C to 24.15°C. This examination provides a thorough understanding of the DCMD system's thermal behavior under various feed inlet temperature conditions.

Figure 15 depicts the effect of the feed inlet mass flow rate on water production on July 21, with this rate ranging from 0.2 kg/s to 1 kg/s. The results show that the behavior of the water flux over time is nearly identical for the various mass flow rates studied and that this flux increases with the feed flow rate. At a flow rate of 1 kg/s, the average flux is 21 kg/m².hr, while at 0.2 kg/s, it is 12.5 kg/m².hr. This figure shows how increasing the flow rate improves the transfer of heat and mass, resulting in more water.

Comparing our findings to previous research, particularly regarding the materials used and daily water production, can provide us with valuable insights and reassurance. As shown in Table 6, our findings are consistent with the literature and demonstrate exemplary water productivity. Our water production rate is 108.56 l/m² mem, which is higher than the other technologies. This good performance confirms that our model has the potential for large-scale solar desalination applications, demonstrating its adaptability and effectiveness in addressing water scarcity challenges. Banat et al. [25] used a 5.73 m² FPC and a 10 m² AGMD module to produce 120 l of water per day at a rate of 12 l/m² for the membrane and 20.73 l/m² for the collector. Bouguecha et al. [52] used a 20 m² FPC and a 3.39 m² DCMD module to produce 18.4 l of water per day. Duong et al.'s [40] simulation study used a larger FPC and 7.2 m² DCMD module, achieving a significant daily water production of 140 l. Asim et al.'s [53] experimental and simulation study found a daily water production of 16 l, with rates of 80 l/m² of membrane and 1.34 l/m² of collector area. These findings imply that various configurations can increase water production efficiency and effectiveness. The simulation involves a 2 m² flat plate collector (FPC) connected

Table 6. Comparison between the current simulation system and the literature studies

Method of study	Solar Collector		Membrane		Daily Production (l)	Water Production (l/m² mem)	Water production (l/m² coll)	References
	Type	Area (m²)	Type	Area (m²)				
Current simulation	FPC	2	DCMD	0.5	54.28	108.56	27.14	-
Experimental	FPC	5.73	AGMD	10	120	12	20.73	[25]
Experimental	FPC	20	DCMD	3.39	18.4	5.43	0.92	[52]
Simulation	FPC	22.6	DCMD	7.2	140	19.4	6.19	[40]
Experimental & Simulation	FPC	11.9	AGMD	0.2	16	80	1.34	[53]

to a 0.5 m² direct contact membrane distillation (DCMD) module. This setup produces 54.28 l of water per day, with a rate of 108.56 l/m² of membrane and 27.14 l/m² of collector area. This finding indicates a positive interaction between the solar collector and the membrane, with the DCMD module efficiently converting heat energy to water.

CONCLUSION

An integrated solar heating system and direct-contact membrane distillation were investigated in this study to generate clean water. This process provides an important solution for regions with insufficient potable water but abundant solar radiation. A literature MATLAB model was adopted, re-coded, and tested in both small and large-scale cases; the mathematical model was based on heat and mass transfer analyses using the membrane and tanks-in-series methods. This model was added as a new component to the TRNSYS simulation by executing an external program. This study used TRNSYS, a transient simulation program, to model solar heating systems, which included a flat plate solar collector and a hot storage tank that powered a DCMD module. Based on time marching, this novel simulation approach uses TRNSYS-MATLAB co-simulation to predict physical phenomena inside the membrane and solar system at the same time, and it was tested throughout the year in Ain Témouchent, Algeria. This dynamic modeling allows for real-time analysis of system parameters. It can be used to investigate several parameters and their effects on solar desalination, including feed and permeate temperatures, feed and permeate flow rates, membrane characteristics (area, porosity, thickness, conductivity), and membrane configurations (co-current and counter-current).

The present DCMD model takes into account all of the parameters. Unlike previous literature approaches to modeling solar desalination (which were very simple), it includes all of the membrane's thermophysical parameters as well as the ability to change its configuration (co-current and counter-current). In comparison to other solar desalination modeling techniques, the current co-simulation allows for more flexibility in predicting different scales and configurations of the MD. It was successfully used in the current study, and the results show good agreement on a small and large scale with literature results for a PVDF flat sheet membrane in two configurations, co-current and counter-current. It was discovered that the counter-current configuration produces more water flow than the co-current configuration, and the difference between the two configurations increases as the membrane area increases. Furthermore, this new technique may enable more precise results, predictive control, and a better-optimized system.

This study assessed solar radiation, useful energy gain, and auxiliary heating rate. The monthly average findings indicate a rise in auxiliary energy consumption. The auxiliary heating rate decreased by approximately 14% in December and 44.27% in August when the collector area was increased from 2 m² to 8 m². In terms of solar system performance over the year, solar fraction (SF) values reached 71%, and solar collector efficiency reached 63% in July. The comparison of the current study to previous research has highlighted the importance of the interaction between solar collector area, membrane type, and module configuration. The current simulation shows competitive water production rates thanks to its balanced FPC and DCMD modules. The findings highlight the potential for efficiently utilizing renewable energy sources for water production, which has practical applications in addressing water scarcity challenges. Consequently, numerous potential applications can be actualized, such as employing this system in diverse environments, including coastal (seawater) and desert areas (brackish water), purifying wastewater, harnessing waste heat, and enhancing system efficiency.

NOMENCLATURE

Symbols

T	Temperature, K
Q_u	Useful thermal energy, kJ/hr
C_p	Specific heat capacity, kJ/kg ·K
$\dot{m}$	Mass flow rate, kg/hr
l_T	Total incident solar radiation, kJ/hr.m²
A_{SC}	Solar collector area, m²
S_F	Solar fraction
Q_{aux}	Auxiliary heating rate, kJ/hr
J	Membrane water flux, kg/m².hr
A	Membrane area, m²
C_m	Water flux permeation coefficient, kg/m²·Pa·s
P	Vapor pressure, Pa
x_{NaCl}	Mole fraction of NaCl in the feed solution
Q_f	Convective heat transfer between the feed and the membrane, W
Q_c	Membrane conductive heat transfer, W
Q_m	Membrane total heat transfer, W
h	Heat transfer coefficient, W/m²·K
ΔH_v	Vaporation latent heat, kJ/kg
k_{mem}	Membrane thermal conductivity, W/m ·K
k_p	Polymer thermal conductivity, W/m ·K
k_g	Vapor thermal conductivity, W/m ·K
D	Hydraulic diameter of a flow channel, m

Greek

η_{coll}	Solar collector efficiency
δ	Thickness, m
ε	Porosity

Subscripts

f	Feed side
p	Permeate side
k	Tank number
m	membrane boundary layer
sat	Saturation
i	The ith point

1	Seawater inlet
2	Solar fluid outlet
3	Solar fluid inlet to the FPC
4	Solar fluid inlet to the coil
5	Seawater outlet position (Feed inlet in the membrane)
6	Feed water outlet
7	Permeate water inlet
8	Permeate water outlet
9	Accumulated distilled water

Abbreviations

MD	Membrane distillation
RO	Reverse osmosis
DCMD	Direct contact membrane distillatio
AGMD	Air-gap membrane distillation
VMD	Vacuum membrane distillation
SGMD	Sweeping gas membrane distillation
FPC	Flat plat collector
CPC	Compound parabolic collector
HTF	Heat transfer fluid
PTFE	Polytetrafluoroethylene
PVDF	Polyvinylidene fluoride
TR-PBOI	Thermally rearranged poly benzoxazole-co -polyimide

ACKNOWLEDGEMENT

The authors express their gratitude to Guangxi Dong for his open-source simulator. We would like to extend our sincere thanks to our friends and family for their support and contributions to the study.

AUTHORSHIP CONTRIBUTIONS

Authors equally contributed to this work.

DATA AVAILABILITY STATEMENT

The authors confirm that the data that supports the findings of this study are available within the article. Raw data that support the finding of this study are available from the corresponding author, upon reasonable request.

CONFLICT OF INTEREST

The authors declared no potential conflicts of interest with respect to the research, authorship, and/or publication of this article.

ETHICS

There are no ethical issues with the publication of this manuscript.

REFERENCES

[1] Yadav A, Labhasetwar PK, Shahi VK. Membrane distillation using low-grade energy for desalination: A review. J Environ Chem Eng 2021;9:105818. [CrossRef]

[2] Rasool M, Banat F. Desalination by solar powered membrane distillation systems. Desalination 2013;308:186-197. [CrossRef]

[3] Tiwari GN, Yadav JK, Singh DB, Al-Helal IM, Abdel-Ghany AM. Exergoeconomic and enviroeconomic analyses of partially covered photovoltaic flat plate collector active solar distillation system. Desalination 2015;367:186-196. [CrossRef]

[4] Hossain F, Miah A, Morshed A, Rabby II, Hu E. Investigation of laminar forced convection heat transfer of nanofluids through flat plate solar collector. J Therm Eng 2021;7:2041-2053. [CrossRef]

[5] Khalifa AE. Flux enhanced water gap membrane distillation process-circulation of gap water. Sep Purif Technol 2020;231:115938. [CrossRef]

[6] Elhenawy Y, Bassyouni M, Fouad K, Sandid AM, Abu-Zeid MAER, Majozi T. Experimental and numerical simulation of solar membrane distillation and humidification - dehumidification water desalination system. Renew Energy 2023;215:118915. [CrossRef]

[7] Panagopoulos A. Beneficiation of saline effluents from seawater desalination plants: Fostering the zero liquid discharge (ZLD) approach - A techno-economic evaluation. J Environ Chem Eng 2021;9:105338. [CrossRef]

[8] Li J, Ren LF, Shao J, Tu Y, Ma Z, Lin Y, et al. Fabrication of triple layer composite membrane and its application in membrane distillation (MD): Effect of hydrophobic-hydrophilic membrane structure on MD performance. Sep Purif Technol 2020;234:116087. [CrossRef]

[9] Phattaranawik J, Jiraratananon R, Fane AG. Heat transport and membrane distillation coefficients in direct contact membrane distillation. J Memb Sci 2003;212:177-193. [CrossRef]

[10] Kebria MRS, Rahimpour A. Membrane distillation: basics, advances, and applications. In: Abdelrasoul A, ed. Advances in Membrane Technologies. IntechOpen; 2020.

[11] Xiong Z, Lai Q, Lu J, Qu F, Yu H, Chen X, et al. Silanization enabled superhydrophobic PTFE membrane with antiwetting and antifouling properties for robust membrane distillation. J Memb Sci 2023;674:121546. [CrossRef]

[12] Teoh MM, Chung TS. Membrane distillation with hydrophobic macrovoid-free PVDF-PTFE hollow fiber membranes. Sep Purif Technol 2009;66:229-236. [CrossRef]

[13] Wang P, Chung TS. Recent advances in membrane distillation processes: Membrane development, configuration design and application exploring. J Memb Sci 2015;474:39-56. [CrossRef]

[14] Chen Y, Lu KJ, Liang CZ, Chung TS. Mechanically strong Janus tri-bore hollow fiber membranes with asymmetric pores for anti-wetting and anti-fouling membrane distillation. Chem Eng J 2022;429:132455. [CrossRef]
[15] Peng N, Widjojo N, Sukitpaneenit P, Teoh MM, Lipscomb GG, Chung TS, et al. Evolution of polymeric hollow fibers as sustainable technologies: Past, present, and future. Prog Polym Sci 2012;37:1401-1424. [CrossRef]
[16] Camacho LM, Dumée L, Zhang J, Li J, Duke M. Advances in membrane distillation for water desalination and purification applications. Water 2013;5:94-196. [CrossRef]
[17] Alkhudhiri A, Darwish N, Hilal N. Membrane distillation: A comprehensive review. Desalination 2012;287:2-18. [CrossRef]
[18] Khayet M. Membranes and theoretical modeling of membrane distillation: A review. Adv Colloid Interface Sci 2011;164:56-88. [CrossRef]
[19] Behnam P, Faegh M, Fakhari I, Ahmadi P, Faegh E, Rosen MA. Thermoeconomic analysis and multi-objective optimization of a novel trigeneration system consisting of kalina and humidification-dehumidification desalination cycles. J Therm Eng 2022;8:52-66. [CrossRef]
[20] Ullah R, Khraisheh M, Esteves RJ, McLeskey JT, AlGhouti M, Gad-el-Hak M, et al. Energy efficiency of direct contact membrane distillation. Desalination 2018;433:56-67. [CrossRef]
[21] Kasaeian A, Babaei S, Jahanpanah M, Sarrafha H, Alsagri AS, Ghaffarian S, et al. Solar humidification-dehumidification desalination systems: A critical review. Energy Convers Manag 2019;201:112129. [CrossRef]
[22] Eddine BT, Salah MM. Solid waste as renewable source of energy: Current and future possibility in Algeria. Waste Manag Valorization Altern Technol 2017;3:115-141. [CrossRef]
[23] Shim WG, He K, Gray S, Moon IS. Solar energy assisted direct contact membrane distillation (DCMD) process for seawater desalination. Sep Purif Technol 2015;143:94-104. [CrossRef]
[24] Ma Q, Xu Z, Wang R. Distributed solar desalination by membrane distillation: Current status and future perspectives. Water Res 2021;198:117154. [CrossRef]
[25] Banat F, Jwaied N, Rommel M, Koschikowski J, Wieghaus M. Desalination by a "compact SMADES" autonomous solarpowered membrane distillation unit. Desalination 2007;217:29-37. [CrossRef]
[26] Fath HES, Elsherbiny SM, Hassan AA, Rommel M, Wieghaus M, Koschikowski J, et al. PV and thermally driven small-scale, stand-alone solar desalination systems with very low maintenance needs. Desalination 2008;225:58-69. [CrossRef]
[27] Banat F, Jwaied N, Rommel M, Koschikowski J, Wieghaus M. Performance evaluation of the "large SMADES" autonomous desalination solar-driven membrane distillation plant in Aqaba, Jordan. Desalination 2007;217:17-28. [CrossRef]
[28] Raluy RG, Schwantes R, Subiela VJ, Peñate B, Melián G, Betancort JR. Operational experience of a solar membrane distillation demonstration plant in Pozo Izquierdo-Gran Canaria Island (Spain). Desalination 2012;290:1-13. [CrossRef]
[29] Selimli S, Recebli Z, Ulker S. Solar vacuum tube integrated seawater distillation - An experimental study. Facta Univ Ser Mech Eng 2016;14:113-20. [CrossRef]
[30] Guillén-Burrieza E, Zaragoza G, Miralles-Cuevas S, Blanco J. Experimental evaluation of two pilot-scale membrane distillation modules used for solar desalination. J Memb Sci 2012;409-410:264-275. [CrossRef]
[31] Schwantes R, Cipollina A, Gross F, Koschikowski J, Pfeifle D, Rolletschek M, et al. Membrane distillation: Solar and waste heat driven demonstration plants for desalination. Desalination 2013;323:93-106. [CrossRef]
[32] Dong G, Kim JF, Hoon J, Drioli E, Moo Y. Open-source predictive simulators for scale-up of direct contact membrane distillation modules for seawater desalination. Desalination 2017;402:72-87. [CrossRef]
[33] Levenspiel O. Comparison of the tanks-in-series and the dispersion models for non-ideal flow of fluid. Chem Eng Sci 1962;17:576-577. [CrossRef]
[34] Yang Q, Lin Q, Sammarchi S, Li J, Li S, Wang D. Water vapor effects on CO2 separation of amine-containing facilitated transport membranes (AFTMs) module: Mathematical modeling using tanks-in-series approach. Greenh Gases Sci Technol 2021;11:52-68. [CrossRef]
[35] Coker DT, Freeman BD, Fleming GK. Modeling multicomponent gas separation using hollow-fiber membrane contactors. AIChE J 1998;44:1289-302. [CrossRef]
[36] Alipour N, Jafari B, Hosseinzadeh K. Optimization of wavy trapezoidal porous cavity containing mixture hybrid nanofluid (water/ethylene glycol Go-Al2O3) by response surface method. Sci Rep 2023;13:1635. [CrossRef]
[37] Remlaoui A, Nehari D, Laissaoui M, Marni A. Performance evaluation of a solar thermal and photovoltaic hybrid system powering a direct contact membrane distillation: TRNSYS simulation. Desalin Water Treat 2020;194:37-51. [CrossRef]
[38] Marni Sandid A, Bassyouni M, Nehari D, Elhenawy Y. Experimental and simulation study of multichannel air gap membrane distillation process with two types of solar collectors. Energy Convers Manag 2021;243:114431. [CrossRef]

[39] Hogan PA, Sudjito, Fane AG, Morrison GL. Desalination by solar heated membrane distillation. Desalination 1991;81:81-90. [CrossRef]
[40] Duong HC, Xia L, Ma Z, Cooper P, Ela W, Nghiem LD. Assessing the performance of solar thermal driven membrane distillation for seawater desalination by computer simulation. J Memb Sci 2017;542:133-142. [CrossRef]
[41] Engel G, Chakkaravarthy AS, Schweiger G. Co-simulation between Trnsys and Simulink based on type155. In: Cerone A, Roveri M, eds. Software Engineering and Formal Methods. SEFM 2017. Lecture Notes in Computer Science, vol 10729. Cham: Springer. pp. 315-329. [CrossRef]
[42] Deshmukh KB, Karmare SV. A review on convective heat augmentation techniques in solar thermal collector using nanofluid. J Therm Eng 2021;7:1257-1266. [CrossRef]
[43] Acevedo L, Uche J, Almo A Del, Círez F, Usón S, Martínez A, et al. Dynamic simulation of a trigeneration scheme for domestic purposes based on hybrid techniques. Energies 2016;9:1013. [CrossRef]
[44] Srimanickam B, Kumar S. Drying investigation of coriander seeds in a photovoltaic thermal collector with solar dryer. J Therm Eng 2023;9:659-668. [CrossRef]
[45] Newton BJ. Modeling of solar storage tanks [Master's Thesis]. University of Wisconsin-Madison; 1995.
[46] Klein SA. TRNSYS 17: A transient system simulation program. Sol Energy Lab Univ Wisconsin 2010;1:1-5.
[47] Hobbi A, Siddiqui K. Optimal design of a forced circulation solar water heating system for a residential unit in cold climate using TRNSYS. Sol Energy 2009;83:700-714. [CrossRef]
[48] Lawson KW, Lloyd DR. Membrane distillation. J Memb Sci 1997;124:1-25. [CrossRef]
[49] Chen TC, Ho CD, Yeh HM. Theoretical modeling and experimental analysis of direct contact membrane distillation. J Memb Sci 2009;330:279-287. [CrossRef]
[50] Perry RH, Green DW. Mass transfer. In: Perry RH, Green DW, eds. Perry's Chemical Engineers' Handbook. 7th ed. New York: Mcgraw-Hill Professional; 1997. pp. 5-59.
[51] Phattaranawik J, Jiraratananon R. Direct contact membrane distillation: Effect of mass transfer on heat transfer. Desalination 2001;188:137-143. [CrossRef]
[52] Bouguecha ST, Aly SE, Al-Beirutty MH, Hamdi MM, Boubakri A. Solar driven DCMD: Performance evaluation and thermal energy efficiency. Chem Eng Res Des 2015;100:331-340. [CrossRef]
[53] Asim M, Uday Kumar NT, Martin AR. Feasibility analysis of solar combi-system for simultaneous production of pure drinking water via membrane distillation and domestic hot water for single-family villa: Pilot plant setup in Dubai. Desalin Water Treat 2016;57:21674-21684. [CrossRef]